



CrossMark  
 click for updates

Cite this: *RSC Adv.*, 2016, 6, 70085

## Efficient deep-blue non-doped organic light-emitting diode with improved roll-off of efficiency based on hybrid local and charge-transfer excited state†

Haichao Liu,<sup>a</sup> Qing Bai,<sup>a</sup> Weijun Li,<sup>b</sup> Yachen Guo,<sup>a</sup> Liang Yao,<sup>a</sup> Yu Gao,<sup>a</sup> Jinyu Li,<sup>a</sup> Ping Lu,<sup>a</sup> Bing Yang<sup>\*a</sup> and Yuguang Ma<sup>c</sup>

High-efficiency deep-blue light-emitting materials are of significance in the fields of commercial full-color displays and solid-state lightings. A hybrid local and charge-transfer (HLCT) excited state not only favors deep-blue emission avoiding a large redshift from a strong charge-transfer (CT) state, but also simultaneously harvests both high photoluminescence efficiency and high exciton-utilizing efficiency. Herein, we report a new V-shaped acceptor–donor–acceptor (A–D–A) type molecule TPA–2PPI with an HLCT emissive state, which is modified from D–A type TPA–PPI. The non-doped device based on the TPA–2PPI emitter still exhibits deep-blue emission peaking at 452 nm with a full width at half maximum (FWHM) of only 50 nm and Commission International de L'Eclairage (CIE) coordinates of (0.151, 0.108). Compared with TPA–PPI, the electroluminescence (EL) not only maintains high efficiency with a maximum external quantum efficiency (EQE) of 4.91%, but also the EL device displays a significantly slower roll-off of efficiency at high luminances with an EQE of 4.89% (or 4.56%) at 100 cd m<sup>-2</sup> (or 1000 cd m<sup>-2</sup>), which is confidently beneficial for the operative stability of OLED devices.

Received 10th June 2016  
 Accepted 18th July 2016

DOI: 10.1039/c6ra15079a

[www.rsc.org/advances](http://www.rsc.org/advances)

### Introduction

Efficient deep-blue light-emitting materials play an irreplaceable role in the field of full-color displays and solid-state lightings.<sup>1</sup> In organic light-emitting diodes (OLEDs), deep-blue materials not only widen the color gamut and reduce power consumption, but also can be utilized as excitation sources to generate other visible and white emissions by an energy cascade.<sup>2</sup> Through persistent efforts, a series of important progresses have been made in the efficiencies of OLEDs in recent years.<sup>3</sup> However, high-efficiency deep-blue OLEDs are really scarce for both phosphorescent and fluorescent types.<sup>4</sup> One of the reasons resulting in low efficiency of deep-blue OLEDs is ascribed to the intrinsic wide bandgap of deep-blue emitter, which is difficult to match the energy levels of functional layers or electrodes in device structure and further causes unbalanced charge injection and charge transport in the electroluminescence (EL) process.<sup>5</sup>

In the past decades, organic donor–acceptor (D–A) type molecules have been gradually constructed to be one of the most commonly-used methods to improve charge injection and carrier transport in organic semiconductor materials.<sup>6</sup> Owing to energy level difference between donor and acceptor, D–A molecule employs the highest occupied molecular orbital (HOMO) of donor and the lowest unoccupied molecular orbital (LUMO) of acceptor to reconstitute proper energy level,<sup>7</sup> in favor of designing device structures with more balanced charge injection and transport. Simultaneously, D–A molecule usually possesses weakly-bound charge transfer (CT) exciton<sup>8</sup> or sufficiently small singlet-triplet energy splitting,<sup>3b–d</sup> which facilitates the reverse intersystem crossing (RISC) process (T → S) to increase triplet exciton-utilizing efficiency of OLEDs. Nevertheless, as inherent CT properties in D–A molecules, the negative effects are also accompanied that CT-state molecule exhibits either a low-efficiency fluorescence due to the forbidden transition induced by the spatially separated hole and electron wavefunctions or a red-shifted emission because of narrowed bandgap, which is disadvantageous for high-efficiency deep-blue emissive materials. In contrast to CT state, locally-excited (LE) state molecule can produce high-efficiency fluorescence due to large oscillator strength from almost complete overlap of hole and electron wavefunctions, and possess non-redshift emission from the small dipole moment of excited state insensitive to the polar environment, which are actually complementary to those of CT state.<sup>7</sup>

<sup>a</sup>State Key Laboratory of Supramolecular Structure and Materials, Jilin University, Changchun, 130012, P. R. China. E-mail: yangbing@jlu.edu.cn

<sup>b</sup>College of Chemical Engineering, Zhejiang University of Technology, Hangzhou, 310014, P. R. China

<sup>c</sup>State Key Laboratory of Luminescent Materials and Devices, South China University of Technology, Guangzhou, 510640, P. R. China

† Electronic supplementary information (ESI) available. See DOI: 10.1039/c6ra15079a

Considering the above issues, if CT and LE states could be integrated into one D–A molecule, it would be an ideal strategy to greatly improve the efficiencies of OLEDs. Recently, hybrid local and charge-transfer (HLCT) excited state<sup>8,9</sup> has been proposed to achieve high-efficiency OLEDs, particularly to meet the challenge between high efficiency and deep-blue emission of OLEDs. In addition, HLCT-state material intrinsically possesses short-lived exciton character, avoiding severe efficiency roll-off from long-lived exciton quenching.<sup>8b</sup> In terms of HLCT state, LE state is introduced to form a new type of excited state with both advantages of LE and CT states, alleviating largely red-shifted emission from strong CT state together with compatible high photoluminescence quantum yield ( $\eta_{\text{PL}}$ ) and high exciton-utilizing efficiency ( $\eta_s$ ). Using HLCT-state conception, high-efficiency deep-blue OLEDs have been obtained in our group, such as a maximum external quantum efficiency (EQE) of 5.02% with a Commission Internationale de L'Eclairage (CIE) coordinate of (0.153, 0.114),<sup>8a</sup> 6.80% with CIE (0.152, 0.077)<sup>4b</sup> and even near ultraviolet emission with EQE of 3.33% and CIE (0.161, 0.049).<sup>8i</sup> Su and Ge also reported HLCT-state molecules, one of whose devices showed violet-blue emission with a maximum EQE of 2.39% and a CIE of (0.16, 0.05).<sup>10</sup> Herein, we report a deep-blue molecule with V-shaped structure, *N*-phenyl-4'-(1-phenyl-1*H*-phenanthro[9,10-*d*]imidazol-2-yl)-*N*-(4'-(1-phenyl-1*H*-phenanthro[9,10-*d*]imidazol-2-yl)-[1,1'-biphenyl]-4-yl)-[1,1'-biphenyl]-4-amine (TPA-2PPI), which is composed of one donor (triphenylamine, TPA) and two acceptors (1,2-diphenyl-1*H*-phenanthro[9,10-*d*]imidazole, PPI), which was derived from TPA-PPI ever reported. It has been demonstrated that TPA acts as donor and PPI as acceptor in TPA-PPI compound.<sup>8a,i,11</sup> In this article, the new type A–D–A molecule is also demonstrated as a typical HLCT-state with two-section different HLCT states. Compared with TPA-PPI, the non-doped TPA-2PPI device also showed a good performance with a maximum EQE of 4.91%, a maximum current efficiency (CE) of 4.76 cd A<sup>-1</sup> and CIE of (0.151, 0.108). Especially, a significantly slower roll-off of efficiency with EQE (or CE) of 4.89% (or 4.74 cd A<sup>-1</sup>) and 4.56% (or 4.42 cd A<sup>-1</sup>) at 100 and 1000 cd m<sup>-2</sup>, respectively.

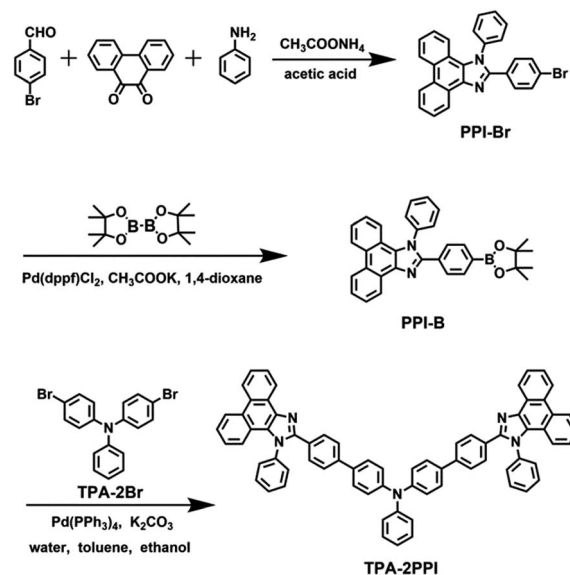
## Results and discussion

### Synthetic procedures

TPA-2PPI was prepared by facile synthesis routes as shown in Scheme 1. PPI-Br was synthesized according to literature<sup>8a</sup>. TPA-2Br and PPI-B were coupled by Suzuki reaction, and crude mixture was purified by chromatography to get target compound. TPA-2PPI was fully characterized and confirmed by <sup>1</sup>H NMR, <sup>13</sup>C NMR, MS and elemental analysis (see ESI†).

### Theoretical calculation

To clearly view molecular conformation of TPA-2PPI, we optimized the ground-state geometry using the density functional theory (DFT) at the level of B3LYP/6-31G(d,p). TPA-2PPI presents a V-shaped conformation with a twist angle of 35° between TPA and PPI moieties for each branch of TPA-2PPI (Fig. S1†).



Scheme 1 Synthetic routes to TPA-2PPI.

Such moderate twist angle does not completely interrupt molecular conjugation between donor (TPA) and acceptor (PPI), and further it is reasonable to construct HLCT state for TPA-2PPI using a proper state coupling between LE and CT. To describe the nature of emission, the lowest singlet state ( $S_1$ ) was optimized using time-dependent DFT theory. As shown in Fig. 1, on the one hand, from the natural transition orbitals (NTO), both hole and particle are mainly delocalized over the molecular backbone and share large overlap. In principle, the NTO of TPA-2PPI well accords with the characteristic of HLCT state. On the other hand, the absorption NTO from hole to particle is mainly related to the transition from HOMO to LUMO, indicating the possible equality of optical and electrical bandgaps (Fig. S2†).

### Photophysical properties

To understand basic photophysical properties of TPA-2PPI, ultraviolet-visible (UV) and photoluminescent (PL) spectra were recorded in both dilute tetrahydrofuran (THF) solution and vacuum-evaporated film (Fig. 2). In THF solution, TPA-2PPI has a long-wavelength absorption band peaked at 374 nm, corresponding to optical bandgap of 2.99 eV estimated from the onset of absorption spectrum. Vacuum-evaporated film of TPA-2PPI has a redshifted absorption peak at 380 nm relative to 374

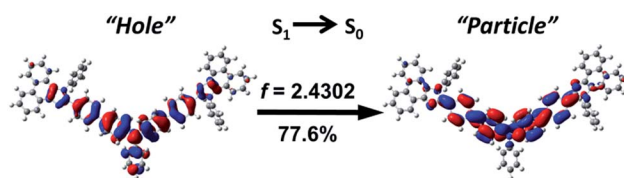


Fig. 1 NTO for  $S_1 \rightarrow S_0$  transition in TPA-2PPI. Herein,  $f$  represents for the oscillator strength, and the percentage weights of hole-particle are given for the  $S_1 \rightarrow S_0$  emission.

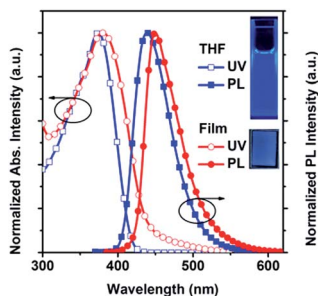


Fig. 2 UV and PL spectra of TPA-2PPI in both THF solution and evaporated film. Insets are the photographs of TPA-2PPI in THF solution and evaporated film, respectively.

nm of TPA-2PPI in THF solution, and also shows a level-off tail in long-wavelength region resulting from molecular aggregation.<sup>12</sup> TPA-2PPI shows deep-blue emission (Fig. 2) in THF solution with a maximum peak at 437 nm and PL efficiency  $\eta_{PL} = 85\%$ . As a contrast, its vacuum-evaporated film has deep-blue emission (Fig. 2) with a slight redshift to 450 nm and  $\eta_{PL} = 50\%$ .

Solvatochromic effect is an inherent property for CT-state molecule,<sup>7</sup> which is commonly used to examine the excited state properties in different solvents. From low-polarity hexane to high-polarity acetonitrile, TPA-2PPI gradually shows broadened PL spectra and vanished vibronic resolution with a redshift of 49 nm from deep blue to pure blue, indicating the existence of CT-state component (Fig. 3a). On the other hand, PL spectra significantly maintain vibrational structures without obvious redshift in low-polarity solvents, demonstrating LE-state component. We applied Lippert–Mataga relation to estimate the dipole moment of excited state ( $\mu_e$ ), describing the variation of excited state of TPA-2PPI. For this purpose, the linear relation of Stokes shift ( $\nu_a - \nu_f$ ) against the orientation polarizability  $f(\epsilon, n)$  was fitted for TPA-2PPI (Fig. 3b and Table S1†). For the vibronic PL spectrum, 0–0 band is chosen as the emission peak to calculate the Stokes shift. The ground-state dipole moment ( $\mu_g$ ) was estimated to be 5.42 D using DFT at the level of B3LYP/6-31G(d,p). As a result, two-section linear relations were well fitted for TPA-2PPI and accordingly two  $\mu_e$ s were estimated to be 10.01 D and 23.27 D, respectively. In low-polarity region,  $\mu_e = 10.01$  D shows a weak CT-state character while  $\mu_e = 23.27$  D indicates a strong CT character in high-polarity region. Most notably, high  $\eta_{PL}$  can be maintained and even slightly raised with the increasing solvent polarity (Fig. 3c), as well as easily distinguished vibronic resolution of PL spectrum in low-polarity solvent clearly demonstrates LE-state character. Thus, both LE and CT states of TPA-2PPI coexist in low-polarity solvents. Furthermore, time-resolved fluorescence reveals a mono-exponential decay of TPA-2PPI in hexane (0.80 ns) and ethyl ether (1.00 ns) (Fig. 3d), which exactly verifies HLCT-state character. In high-polarity region,  $\mu_e = 23.27$  D of TPA-2PPI is almost equal to that of 4-(*N,N*-dimethylamino) benzonitrile (DMABN), which is a typical CT molecule with a  $\mu_e = 23$  D.<sup>7</sup> It can be inferred that TPA-2PPI possesses CT-dominated state character in high-polarity solvents. It is well-known that strong CT-state molecule suffers from the sharply

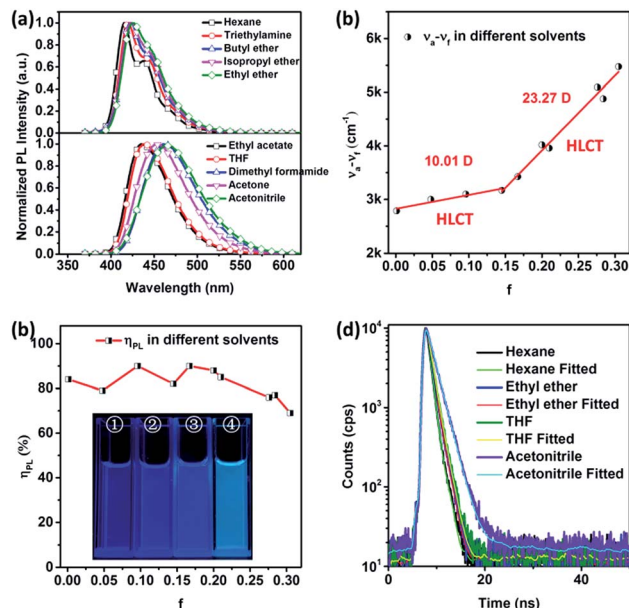


Fig. 3 (a) Solvatochromic PL spectra of TPA-2PPI with the increased solvent polarity. (b) Linear fitting of Lippert–Mataga model (the semi-solid circles represent the Stokes shifts in different solvents, and the lines are fitted for solvatochromic model). (c)  $\eta_{PL}$ s of TPA-2PPI with the increased solvent polarity. Insets are the photographs of TPA-2PPI in four different solutions (hexane, ethyl ether, THF and acetonitrile successively from serial number 1 to 4). (d) Time-resolved fluorescence of TPA-2PPI in hexane, ethyl ether, THF and acetonitrile.

declined  $\eta_{PL}$  as solvent polarity increases. However, the  $\eta_{PL}$ s of TPA-2PPI still remain at high level and mildly decline with the increasing solvent polarity, and even  $\eta_{PL} = 69\%$  in high-polarity acetonitrile, which should be attributed to a certain degree of LE state component. Time-resolved fluorescence also reveals a mono-exponential decay of TPA-2PPI in THF (1.08 ns) and acetonitrile (1.68 ns), indicating that TPA-2PPI possesses the HLCT-state character in high-polarity solvents. Given this, the process from low to high polarity can be divided into two stages: LE-dominated low-polarity region and CT-dominated high-polarity region respectively for the HLCT state of TPA-2PPI. That is, TPA-2PPI maintains the HLCT-state character all the time from low-polarity hexane to high-polarity acetonitrile.

To check the photostability of TPA-2PPI material, we collected the <sup>1</sup>H NMR spectra after the sample dissolving in deuterated dimethylsulphoxide (DMSO) solvent was irradiated for different time under 365 nm UV irradiation. All <sup>1</sup>H NMR spectra are consistent (Fig. S3†), demonstrating the photostability of TPA-2PPI material, *i.e.*, unchanged molecular structure of TPA-2PPI compound after UV irradiation.

### Thermal and electrochemical properties

The thermal properties were investigated by differential scanning calorimetry (DSC) and thermogravimetric analysis (TGA), which demonstrates that A–D–A type TPA-2PPI is highly thermally stable. The glass transition temperature ( $T_g$ ) and thermal decomposition temperature ( $T_d$ ) were measured as 201 °C and 576 °C respectively (Fig. S4†), which are very high probably due

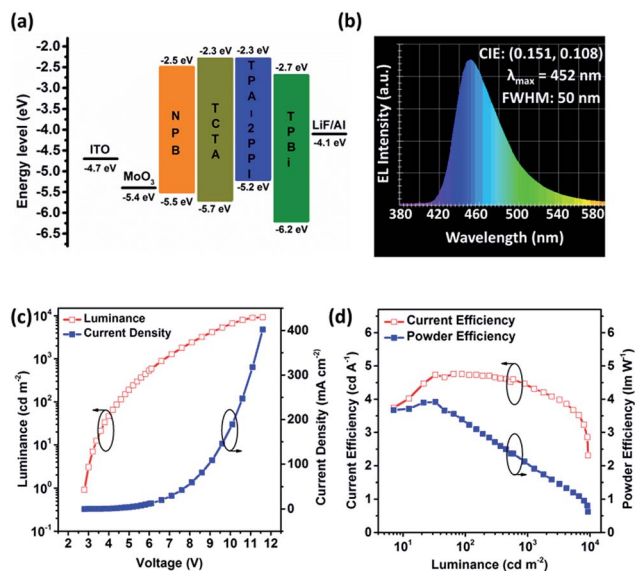


Fig. 4 (a) Schematic energy level diagram of TPA-2PPI device. (b) EL spectrum of TPA-2PPI device. (c) Luminance-voltage-current density curves. (d) Current efficiency-luminance-powder efficiency curves.

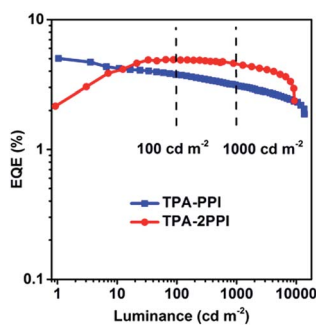


Fig. 5 EQE-luminance curves of TPA-PPI and TPA-2PPI devices.

to the larger molecular dimension of TPA-2PPI. To further ensure the thermal stability of TPA-2PPI material, we annealed TPA-2PPI powder at 360 °C. Compared with the prepared solid powder after column chromatography, both  $^1\text{H}$  NMR spectra are identical (Fig. S5<sup>†</sup>), demonstrating the unchanged structure and the excellent thermal stability after annealing TPA-2PPI powder. Cyclic voltammetry (CV) were measured to calculate the HOMO and LUMO levels of  $-5.19$  eV and  $-2.29$  eV, respectively (Fig. S4<sup>†</sup>). Correspondingly, the electrical bandgap of TPA-2PPI

was estimated to be 2.90 eV, which is almost the same as 2.99 eV of optical bandgap, as predicted by theoretical calculation.

### Electroluminescence properties

In order to investigate the EL property, TPA-2PPI serves as emitter to construct the multi-layer non-doped device (Fig. 4a): ITO/MoO<sub>3</sub> (7 nm)/NPB (50 nm)/TCTA (10 nm)/TPA-2PPI (20 nm)/TPBi (40 nm)/LiF (1 nm)/Al (120 nm), in which NPB = *N,N'*-di-1-naphthyl-*N,N'*-diphenylbenzidine, TCTA = 4,4',4''-tri(*N*-carbazolyl)-triphenylamine, TPBi = 1,3,5-tri(phenyl-2-benzimidazolyl)-benzene. MoO<sub>3</sub> was utilized as a hole-injecting layer, NPB and TCTA as hole-transporting and buffer layers, and TPBi as an electron-transporting and hole-blocking layer. Deep-blue emission was observed, and EL spectrum is peaked at 452 nm with a full width at half maximum (FWHM) of only 50 nm and CIE coordinate of (0.151, 0.108) (Fig. 4b). Narrow FWHM contributes to good CIE chromaticity of TPA-2PPI device. Fig. 4c shows the luminance-voltage-current density characteristics of the device. TPA-2PPI device has a very low turn-on voltage of 2.8 V at 1  $\text{cd m}^{-2}$ , which is ascribed to well-matched energy level alignment in the device. Moreover, the EL spectra of the TPA-2PPI device are surely independent of driving voltages from 3 V to 11 V, revealing that the recombination of electrons and holes is well confined within the emitter layer during the EL process (Fig. S6<sup>†</sup>).

TPA-2PPI device shows a good performance with a maximum EQE, a maximum CE and a maximum power efficiency (PE) of 4.91% (at 4.2 V and 65  $\text{cd m}^{-2}$ ), 4.76  $\text{cd A}^{-1}$  and 3.61  $\text{lm W}^{-1}$ , respectively (Fig. 4d and 5). The maximum luminance reaches to 9277  $\text{cd m}^{-2}$ , and particularly, the device has a very low roll-off of EQE and CE with the enhanced luminance. In terms of the practical applications, between 100 and 1000  $\text{cd m}^{-2}$ , EQE (or CE) can be maintained at 4.89% (or 4.74  $\text{cd A}^{-1}$ ) and 4.56% (or 4.42  $\text{cd A}^{-1}$ ), as shown in Table 1. Furthermore, the  $\eta_s$  can be roughly estimated for TPA-2PPI devices on the basis of the known  $\eta_{\text{PL}}$  value, maximum EQE and the other two assumed parameters of the light out-coupling efficiency of 20% and the 100% hole-electron recombination in the OLEDs. Thus, the  $\eta_s = 49\%$  in the TPA-2PPI device is obtained, which breaks through the upper-limit of  $\eta_s = 25\%$  in the conventional fluorescent OLEDs, which can be attributed to the HLCT-state and hot exciton mechanism, indicating a harmony between high  $\eta_{\text{PL}}$  (50%) and high  $\eta_s$  (49%).

As a comparison, TPA-PPI as a typical deep-blue molecule whose device exhibited excellent performance with a maximum EQE of 5.02%, a maximum CE of 5.66  $\text{cd A}^{-1}$  and CIE coordinate

Table 1 Electroluminescent characteristics of TPA-PPI and TPA-2PPI devices

	$\lambda_{\text{EL,max}}$ (nm)	CIE (x, y)	$\text{CE}_{\text{max}}$ ( $\text{cd A}^{-1}$ )	$\text{PE}_{\text{max}}$ ( $\text{lm W}^{-1}$ )	$\text{EQE}_{\text{max}}$ (%)	$I_{\text{max}}$ ( $\text{cd m}^{-2}$ )	@100 $\text{cd m}^{-2}$			@1000 $\text{cd m}^{-2}$		
							CE ( $\text{cd A}^{-1}$ )	PE ( $\text{lm W}^{-1}$ )	EQE (%)	CE ( $\text{cd A}^{-1}$ )	PE ( $\text{lm W}^{-1}$ )	EQE (%)
TPA-2PPI	452	(0.151, 0.108)	4.76	3.61	4.91	9277	4.74	3.30	4.89	4.42	2.04	4.56
TPA-PPI	434	(0.153, 0.114)	5.66	6.13	5.02	13 675	4.25	2.70	3.76	3.50	1.39	3.13

of (0.153, 0.114), has been reported by our group in 2012.<sup>8a</sup> Although A–D–A type TPA–2PPI and D–A type TPA–PPI share almost the same device performance, TPA–2PPI device exhibits the slower roll-off of efficiency (Table 1 and Fig. 5) and the more stable thermal property than those of TPA–PPI, which may jointly contribute to the better final device operative stability. As a whole, TPA–2PPI device is still the one among the best deep-blue fluorescent OLEDs.

## Conclusions

A V-shaped molecule TPA–2PPI was synthesized with one donor and two acceptors, which was modified from D–A type TPA–PPI. TPA–2PPI shows HLCT-state property from low-polarity hexane to high-polarity acetonitrile, although two-section linear relations were well fitted by Lippert–Mataga equation. Moreover, its thermal stability is greatly improved relative to TPA–PPI. The non-doped device based on TPA–2PPI emitter exhibits deep-blue EL spectrum peaked at 452 nm with a FWHM of only 50 nm and CIE coordinates of (0.151, 0.108). The device shows excellent performance with a maximum EQE of 4.91% and a maximum CE of 4.76 cd A<sup>-1</sup>. Moreover, the device also presents very slow roll-off of EQE (or CE), which can be maintained at 4.89% (or 4.74 cd A<sup>-1</sup>) and 4.56% (or 4.42 cd A<sup>-1</sup>) at a practical range between 100 and 1000 cd m<sup>-2</sup>. This work not only proposes an idea to design high-efficiency deep-blue OLED materials using HLCT mechanism, but also provides a feasible way to enhance the OLED device stability with the increased thermal stability and the slower roll-off of efficiency and without the sacrifice of efficiency and CIE coordinate using the modified ratio of D and A.

## Acknowledgements

This work was supported by the National Natural Science Foundation of China (51273078, 51473063 and 91233113), the Ministry of Science and Technology of China (2013CB834801 and 2015CB655003) and the Open Project Foundation of the State Key Laboratory of Luminescence and Applications (Changchun Institute of Optics, Fine Mechanics and Physics of the Chinese Academy of Science, SKLA-2016-04).

## Notes and references

- (a) X. Yang, X. Xu and G. Zhou, *J. Mater. Chem. C*, 2015, **3**, 913; (b) M. Zhu and C. Yang, *Chem. Soc. Rev.*, 2013, **42**, 4963; (c) J. Kwak, J. Lim, M. Park, S. Lee, K. Char and C. Lee, *Nano Lett.*, 2015, **15**, 3793; (d) H. Shen, X. Bai, A. Wang, H. Wang, L. Qian, Y. Yang, A. Titov, J. Hyonen, Y. Zheng and L. S. Li, *Adv. Funct. Mater.*, 2014, **24**, 2367; (e) Z. Yuan, Y. Shu, Y. Tian, Y. Xin and B. Ma, *Chem. Commun.*, 2015, **51**, 16385; (f) K.-H. Lee, J.-H. Lee, W.-S. Song, H. Ko, C. Lee, J.-H. Lee and H. Yang, *ACS Nano*, 2013, **7**, 7295.
- (a) H. Xiao, L. Ding, D. Ruan, B. Li, N. Ding and D. Ma, *Dyes Pigm.*, 2015, **121**, 7; (b) G. Schwartz, M. Pfeiffer, S. Reineke, K. Walzer and K. Leo, *Adv. Mater.*, 2007, **19**, 3672; (c) S. J. Lee, J. S. Park, K.-J. Yoon, Y.-I. Kim, S.-H. Jin, S. K. Kang, Y.-S. Gal, S. Kang, J. Y. Lee, J.-W. Kang, S.-H. Lee, H.-D. Park and J.-J. Kim, *Adv. Funct. Mater.*, 2008, **18**, 3922; (d) L. S. Hung and C. H. Chen, *Mater. Sci. Eng., R*, 2002, **39**, 143; (e) Z. Zhang, W. Jiang, X. Ban, M. Yang, S. Ye, B. Huang and Y. Sun, *RSC Adv.*, 2015, **5**, 29708.
- (a) M. A. Baldo, D. F. O'Brien, Y. You, A. Shoustikov, S. Sibley, M. E. Thompson and S. R. Forrest, *Nature*, 1998, **395**, 151; (b) H. Uoyama, K. Goushi, K. Shizu, H. Nomura and C. Adachi, *Nature*, 2012, **492**, 234; (c) Q. Zhang, B. Li, S. Huang, H. Nomura, H. Tanaka and C. Adachi, *Nat. Photonics*, 2014, **8**, 326; (d) Y. Tao, K. Yuan, T. Chen, P. Xu, H. H. Li, R. F. Chen, C. Zheng, L. Zhang and W. Huang, *Adv. Mater.*, 2014, **26**, 7931.
- (a) W. Qin, Z. Yang, Y. Jiang, J. W. Y. Lam, G. Liang, H. S. Kwok and B. Z. Tang, *Chem. Mater.*, 2015, **27**, 3892; (b) X. Tang, Q. Bai, Q. Peng, Y. Gao, J. Li, Y. Liu, L. Yao, P. Lu, B. Yang and Y. Ma, *Chem. Mater.*, 2015, **27**, 7050; (c) L. Li, B. Jiao, Y. Yu, L. Ma, X. Hou and Z. Wu, *RSC Adv.*, 2015, **5**, 59027.
- (a) J.-Y. Hu, Y.-J. Pu, F. Satoh, S. Kawata, H. Katagiri, H. Sasabe and J. Kido, *Adv. Funct. Mater.*, 2014, **24**, 2064; (b) M.-J. Kim, C.-W. Lee and M.-S. Gong, *Org. Electron.*, 2014, **15**, 2922; (c) C.-H. Chien, C.-K. Chen, F.-M. Hsu, C.-F. Shu, P.-T. Chou and C.-H. Lai, *Adv. Funct. Mater.*, 2009, **19**, 560; (d) G. Malleshham, C. Swetha, S. Niveditha, M. E. Mohanty, N. J. Babu, A. Kumar, K. Bhanuprakash and V. J. Rao, *J. Mater. Chem. C*, 2015, **3**, 1208; (e) W. Hua, Z. Liu, L. Duan, G. Dong, Y. Qiu, B. Zhang, D. Cui, X. Tao, N. Cheng and Y. Liu, *RSC Adv.*, 2015, **5**, 75; (f) W.-C. Chen, G.-F. Wu, Y. Yuan, H.-X. Wei, F.-L. Wong, Q.-X. Tong and C.-S. Lee, *RSC Adv.*, 2015, **5**, 18067.
- (a) Y. Shirota, M. Kinoshita, T. Noda, K. Okumoto and T. Ohara, *J. Am. Chem. Soc.*, 2000, **122**, 11021; (b) H. Doi, M. Kinoshita, K. Okumoto and Y. Shirota, *Chem. Mater.*, 2003, **15**, 1080.
- Z. R. Grabowski, K. Rotkiewicz and W. Rettig, *Chem. Rev.*, 2003, **103**, 3899.
- (a) W. Li, D. Liu, F. Shen, D. Ma, Z. Wang, T. Feng, Y. Xu, B. Yang and Y. Ma, *Adv. Funct. Mater.*, 2012, **22**, 2797; (b) S. Zhang, W. Li, L. Yao, Y. Pan, F. Shen, R. Xiao, B. Yang and Y. Ma, *Chem. Commun.*, 2013, **49**, 11302; (c) W. Li, Y. Pan, R. Xiao, Q. Peng, S. Zhang, D. Ma, F. Li, F. Shen, Y. Wang, B. Yang and Y. Ma, *Adv. Funct. Mater.*, 2014, **24**, 1609; (d) Y. Pan, W. Li, S. Zhang, L. Yao, C. Gu, H. Xu, B. Yang and Y. Ma, *Adv. Opt. Mater.*, 2014, **2**, 510; (e) W. Li, Y. Pan, L. Yao, H. Liu, S. Zhang, C. Wang, F. Shen, P. Lu, B. Yang and Y. Ma, *Adv. Opt. Mater.*, 2014, **2**, 892; (f) L. Yao, S. Zhang, R. Wang, W. Li, F. Shen, B. Yang and Y. Ma, *Angew. Chem., Int. Ed.*, 2014, **53**, 2119; (g) S. Zhang, L. Yao, Q. Peng, W. Li, Y. Pan, R. Xiao, Y. Gao, C. Gu, Z. Wang, P. Lu, F. Li, S. Su, B. Yang and Y. Ma, *Adv. Funct. Mater.*, 2015, **25**, 1755; (h) L. Yao, Y. Pan, X. Tang, Q. Bai, F. Shen, F. Li, P. Lu, B. Yang and Y. Ma, *J. Phys. Chem. C*, 2015, **119**, 17800; (i) H. Liu, Q. Bai, L. Yao, H. Zhang, H. Xu, S. Zhang, W. Li, Y. Gao, J. Li, P. Lu, H. Wang, B. Yang and Y. Ma, *Chem. Sci.*, 2015, **6**, 3797.

- 9 D. Fan, Y. Yi, Z. Li, W. Liu, Q. Peng and Z. Shuai, *J. Phys. Chem. A*, 2015, **119**, 5233.
- 10 X. Ouyang, X.-L. Li, X. Zhang, A. Islam, Z. Ge and S.-J. Su, *Dyes Pigm.*, 2015, **122**, 264.
- 11 Y. Zhang, S.-L. Lai, Q.-X. Tong, M.-F. Lo, T.-W. Ng, M.-Y. Chan, Z.-C. Wen, J. He, K.-S. Jeff, X.-L. Tang, W.-M. Liu, C.-C. Ko, P.-F. Wang and C.-S. Lee, *Chem. Mater.*, 2012, **24**, 61.
- 12 J. Luo, Z. Xie, J. W. Y. Lam, L. Cheng, B. Z. Tang, H. Chen, C. Qiu, H. S. Kwok, X. Zhan, Y. Liu and D. Zhu, *Chem. Commun.*, 2001, 1740.